ACS SENSORS

pubs.acs.org/acssensors Article

SABRE-SHEATH Hyperpolarization of [1,5-$^{13}C_2$]Z-OMPD for Noninvasive pH Sensing

Mustapha B. Abdulmojeed,* Martin Grashei, Seth Dilday, Pascal Wodtke, Stephen McBride, Atli Davidsson, Erica Curran, Keilian MacCulloch, Austin Browning, Patrick TomHon, Andreas B. Schmidt, Eduard Y. Chekmenev, Franz Schilling, and Thomas Theis*

Cite This: https://doi.org/10.1021/acssensors.4c01102 Read Online

ACCESS | Metrics & More | Article Recommendations | Supporting Information

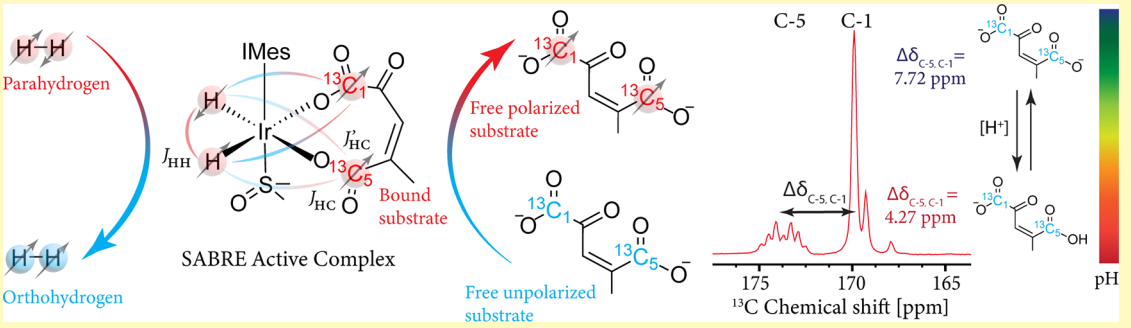

ABSTRACT: Hyperpolarized (HP) ^{13}C-labeled probes are emerging as promising agents to noninvasively image pH in vivo. HP [1,5-$^{13}C_2$]Z-OMPD (Z-4-methyl-2-oxopent-3-enedioic acid) in particular has recently been used to simultaneously report on kidney perfusion, filtration, and pH homeostasis, in addition to the ability to detect local tumor acidification. In previous studies, dissolution dynamic nuclear polarization was used to hyperpolarize Z-OMPD. Here, we pioneered the hyperpolarization of [1,5-$^{13}C_2$]Z-OMPD via SABRE-SHEATH (signal amplification by reversible exchange in shield enabling alignment transfer to heteronuclei), which is relatively simple and fast and promises to be highly scalable. With SABRE-SHEATH, we achieve enhancement values of ∼3950 and ∼2400 at 1.1 T (P_{13C} = 0.4 and 0.25%) on the labeled C-1 and C-5 positions of Z-OMPD. Density functional theory calculations at the B3LYP level of theory were used to investigate possible binding modes of Z-OMPD on the iridium-based polarization transfer catalyst. The experimental and theoretical results suggest that the equatorial binding mode to the catalyst, where Z-OMPD binds to the catalyst at both C-1 and C-5 carboxylate positions, is the most stable complex. The HP signals were used to measure the Z-OMPD chemical shift as a function of pH showing an ∼3 ppm shift across pH 4−11. This work lays a foundation for the development of a simple, low-cost hyperpolarization technique to image pH.

KEYWORDS: *NMR, hyperpolarization, [1,5-$^{13}C_2$]Z-OMPD, SABRE-SHEATH, pH sensing*

Extracellular pH is a tissue characteristic, which is altered in multiple pathological states such as in cancer,[1−7] ischemia,[8−10] chronic obstructive pulmonary disease,[11] and renal tubular acidosis.[10,12] Here, acidification is not only a disease hallmark but also has a significant impact on the treatment outcome, e.g., of tumors.[13] Modern treatments, such chemotherapeutics[14] or engineered T cells,[15] are highly susceptible to the pH of the target tissue. It has been shown that treatment efficacy can be enhanced, when pH-conditioning adjuvant therapies are employed prior to the main therapy.[16−19] To timely adjust these treatment steps, noninvasive monitoring of the tissue pH is key. Magnetic resonance (MR) methods can provide accurate and precise noninvasive measurement of pH in vivo with reasonable spatial resolution.[20−24] A promising MR-based method takes advantage of changes in chemical shifts due to changes in the local electronic environment induced by pH-driven proton exchange. An ideal MR pH sensor should have the following properties: (1) large pH sensitivity, (2) a pK_a in the physiological range, (3) no toxicity at concentrations obtained in vivo after injection, (4) metabolic stability, and (5) high sensitivity (high signal-to-noise ratio).[25] Common MR pH sensors such as 3-aminopropylphosphonate (3-APP)[26] and 2-imidazole-1-yl-3 ethoxycarbonylpropionic acid[27] satisfy most of these conditions but are limited due to low sensitivity and overlap with background signals.[28−31]

Received: May 8, 2024
Revised: October 17, 2024
Accepted: October 21, 2024

The challenge of background signals can be mitigated using carbon-13-labeled MR pH sensors. Unfortunately, ^{13}C nuclei have low natural abundance (1.1%) and low gyromagnetic ratio (four times lower than that of ^{1}H). Additionally, MR methods are generally less sensitive compared to other techniques, such as optical and electrochemical methods. This low sensitivity is due to the intrinsically low net magnetization of the nuclear spins even at high magnetic field.[32,33] The sensitivity issue can be tackled by using isotopically enriched ^{13}C pH sensors in combination with hyperpolarization, which increases the net magnetization of the spins by several orders of magnitude.[34−37]

[1,5-$^{13}C_2$]Z-OMPD, hereafter referred to as Z-OMPD, has been introduced as a promising hyperpolarized (HP) MR-based pH probe as the chemical shifts of C-1 and C-5 have strong sensitivity to pH.[38] Furthermore, Z-OMPD (structure shown in Figure 1A) appears to be nontoxic and metabolically stable.[38] The pK_a values of the C-1 and C-5 carboxylates are <3 and 6.55 (in water), respectively. The pK_a of 6.55 is in the physiological range, making Z-OMPD a well-suited MR pH sensor. In addition, both C1 and C5 exhibit long T_1 in vivo (~30 s at 7 T). Moreover, the C-1 resonance serves as an internal chemical shift reference for pH determination. Recent work used Z-OMPD hyperpolarized with dissolution dynamic nuclear polarization (d-DNP) to measure extracellular pH and perfusion. That previous study provided multiparametric fingerprints of renal disease and allowed the detection of local tumor acidification.[38]

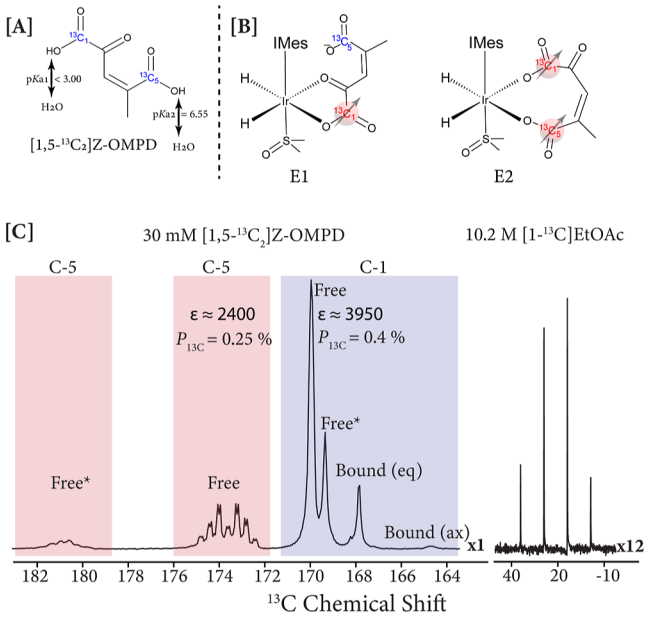

Figure 1. (A) 2D structure of Z-OMPD indicating the labeling of the HP carbons. (B) Dominant binding modes of Z-OMPD to the Ir-IMes catalyst. In E1, Z-OMPD binds equatorially via oxo groups at C-1 and C-2 (E1). In E2, Z-OMPD binds via the oxo groups at C-1 and C-5 (E2). (C) Left: ^{13}C NMR spectra of HP [1,5-^{13}C-2]Z-OMPD peaks showing both free C-1 and C-5 peaks and equatorial and axial bound C-1 peaks (peaks in asterisk are not fully identified). Right: ^{13}C NMR spectrum of thermally polarized 10.2 M [1-^{13}C]ethyl acetate. Both spectra were detected at 1.1 T benchtop NMR spectrometer (Spinsolve Carbon, Magritek). The enhancements, ε, are relative to thermal measurements at 1.1 T.

For the present study, we show for the first time that signal amplification by reversible exchange in shield enabling alignment transfer to heteronuclei (SABRE-SHEATH)[39,40] can hyperpolarize [1,5-$^{13}C_2$]Z-OMPD, as illustrated in Figure 1. Signal amplification by reversible exchange (SABRE) is a parahydrogen-based HP method that relies on the reversible exchange of parahydrogen and a target substrate[41] on an organometallic catalyst ([Ir(H_2)(IMes)(Substrate)$_n$]).[42] Polarization transfer during SABRE, from parahydrogen to the target nuclei on the substrate, is achieved when the frequency difference between source and target nuclei match the spin−spin J-coupling interaction between the two parahydrogen-derived hydrides on the catalyst.[39,40,43] Accordingly, polarization transfer to heteronuclei such as ^{13}C, ^{15}N, and ^{31}P is best accomplished at microtesla fields.[44−46] To establish microtesla fields, we use μ-metal to shield the system from the earth's magnetic field. This so-called SABRE-SHEATH approach allows the polarization of a wide range of biologically relevant molecules and directly hyperpolarizes the long-lived heteronuclear sites, associated with long T_1, enabling longer metabolic tracking. Though SABRE-SHEATH is limited in terms of substrate scope and polarization levels when compared to more widely used d-DNP methods, the technology package required for SABRE-SHEATH is compact, fast, and easy to set up.[41,47−50] In recent years, the hyperpolarization of the central HP MRI agent, pyruvate, has also attracted much attention.[51−53]

Here, we demonstrate the use of SABRE-SHEATH to hyperpolarize both the C-1 and C-5 resonances of the pH sensing molecule [1,5-$^{13}C_2$]Z-OMPD. We find that multiple binding modes are responsible for polarization transfer (Figure 1B) detailed under Results and Discussion. The work highlights the versatility of SABRE-SHEATH in polarizing multiple nuclei in one molecule simultaneously (Figure 1C), showing enhancements of >2000 fold over thermal reference measurements at 1.1 T (P_{13C} > 0.25%) for C-5, and almost 4000-fold enhancement for C-1 (P_{13C} > 0.4%). Even though this polarization does not reach levels favorable for in vivo application (>10% required), further optimization is likely to improve hyperpolarization levels in the future. One opportunity is the use of SLIC-SABRE,[54−56] which in some cases outperforms SABRE-SHEATH. In addition, we also use ab initio density functional theory (DFT) calculations to examine the binding mechanisms of Z-OMPD to the catalyst, rationalizing experimental observations. Finally, we experimentally verify the pH sensing ability of HP Z-OMPD by measuring the chemical shifts of C-1 and C-5 as a function of pH across the physiological pH range.

MATERIALS AND METHODS

The standard SABRE precatalyst [Ir(IMes)(COD)Cl] [IMes = 1,3 bis(2,4,6-trimethylphenyl)imidazole-2-ylidene, COD = cyclooctadiene] was synthesized according to a previously established procedure.[42] Z-OMPD was synthesized by aldol reaction of [1-^{13}C]ethyl pyruvate in a methanolic sodium hydroxide solution followed by acid hydrolysis and prep-HPLC purification as reported by Grashei et al.[38,57] CD_3OD was purchased from Cambridge Isotopes Laboratories, Inc., degassed with three freeze−pump−thaw cycles, and stored under argon. All other chemicals were purchased from Millipore and used without further purification.

Sample Preparation for SABRE-SHEATH Experiments. Each experiment in this manuscript was conducted with a standard sample of 0.7 mL of methanol solution containing 6 mM precatalyst ([Ir(IMes)(COD)Cl]), 20 mM dimethyl sulfoxide (DMSO), and 30

https://doi.org/10.1021/acssensors.4c01102
ACS Sens. XXXX, XXX, XXX−XXX

mM Z-OMPD adjusted to pH 8.42 by adding up to 35 mM solution of NaOD in D_2O as measured with a pH meter [pH measurements were performed using a SevenDirect SD23 pH/conductivity meter with InLab Micro ProISM (51344163)]. This solution was degassed with argon before transfer to a 5 mm medium-walled NMR tube fitted with a 1/4 in. outer-diameter (OD) Teflon tube extension and connected to a parahydrogen (pH_2) bubbling set up through a Wye 1/8 in. to 1/4 in. push-to-connect fitting. Details about the setup are described elsewhere.[58]

The sample was activated for 10 min at 0 °C by bubbling ~98% pH_2 at 100 psi. For each experiment, the temperature cycling method was adopted.[59] The solution was first precooled to 0 °C for a minute, placed in a polarization transfer field (PTF) of 0.4 μT, and bubbled at room temperature (~20 °C) with a flow rate of 120 sccm. After 30 s, the bubbling was stopped and the sample was quickly transported (2−3 s) to a 1.1 T benchtop spectrometer (Spinsolve Carbon, Magritek) for detection. All experiments were carried out with this protocol, except when stated otherwise. The ^{13}C polarization (P_{13C}) was calculated using a thermally polarized sample of neat (~10.2 M) [1-^{13}C]ethyl acetate as a reference (see Supporting Information).

All DFT calculations of the SABRE complexes were conducted using the Gaussian 16 package[60] installed on the NCSU high-performance computer (Hazel). DFT geometry optimization was performed at the B3LYP[61−64] level of theory with a D3 dispersion correction and the 6-311g (d) basis set for C, O, N, and S atoms. Iridium was modeled with the Stuttgart-Dresden effective core potential and its associated basis from the GENECP key word within Gaussian with an f-polarization function derived from Ehlers et al.[65,66] (see Supporting Information).

RESULTS AND DISCUSSION

In the presented experiments, we employed the temperature cycling procedure described above. The underlying principle of this approach is to allow maximum initial polarization buildup on the catalyst-bound substrate at low temperatures associated with slower exchange rates. This procedure takes advantage of the relatively slow exchange of Z-OMPD compared to that of the hydrides at low temperature (0 °C). After precooling, bubbling at room temperature (20 °C) leads to gradual release of the bound species into its free form as the temperature of the sample slowly increases. Figure 1C shows a spectrum of HP Z-OMPD obtained by using this approach. C-1 (~170 ppm) and C-5 (~175 ppm) show enhancements (ε) of ~3950 and ~2400, respectively, corresponding to P_{13C} of 0.4% for C-1 and 0.25% for C-5. The observed splitting on the C-5 peaks is due to coupling to nearby protons.

The observed splitting could be removed through either decoupling or deuteration. The peaks marked with asterisks have not been fully identified. We believe that they correspond to free Z-OMPD isomers in solution because the temperature-dependent data shows increasing intensity of these peaks with increasing temperature, as detailed in Supporting Information Figure S2.

As illustrated in Scheme 1, Z-OMPD (Scheme 1a) has an alpha-keto acid functional moiety and can be expected to exhibit similar SABRE chemistry as pyruvate, a well-studied alpha-keto acid substrate in SABRE hyperpolarization.[59,67−71] Based on the known pyruvate binding modes, we first expected that, upon activation of the precatalyst in the presence of DMSO, Z-OMPD, and pH_2, at least two activated SABRE complexes are formed.[67] The first complex is equatorial complex E1 (Scheme 1a) in which Z-OMPD coordinates equatorially to the iridium center through the carboxylate and keto groups in positions 1 and 2, respectively. The second is the axial complex **A1** (Scheme 1a), in which coordination occurs axially. For comparison with previous works[67,70]

Scheme 1. (A) Activation of [IrIMes(COD)Cl] in the Presence of DMSO, Parahydrogen, and Z-OMPD to Form the SABRE Active Equatorial Complexes E1 and E2 and Axial Complexes A1 and A2; the DMSO Complex ($[Ir(H)_2(DMSO)_2(IMES)Cl]$), Which Enhances pH_2 Exchange, Is Also Formed in the Process; (B) Reversible Exchange of Parahydrogen and Z-OMPD via the SABRE Active Complex E1; (C) Reversible Exchange of Parahydrogen and Z-OMPD via the SABRE-Active Complex E2

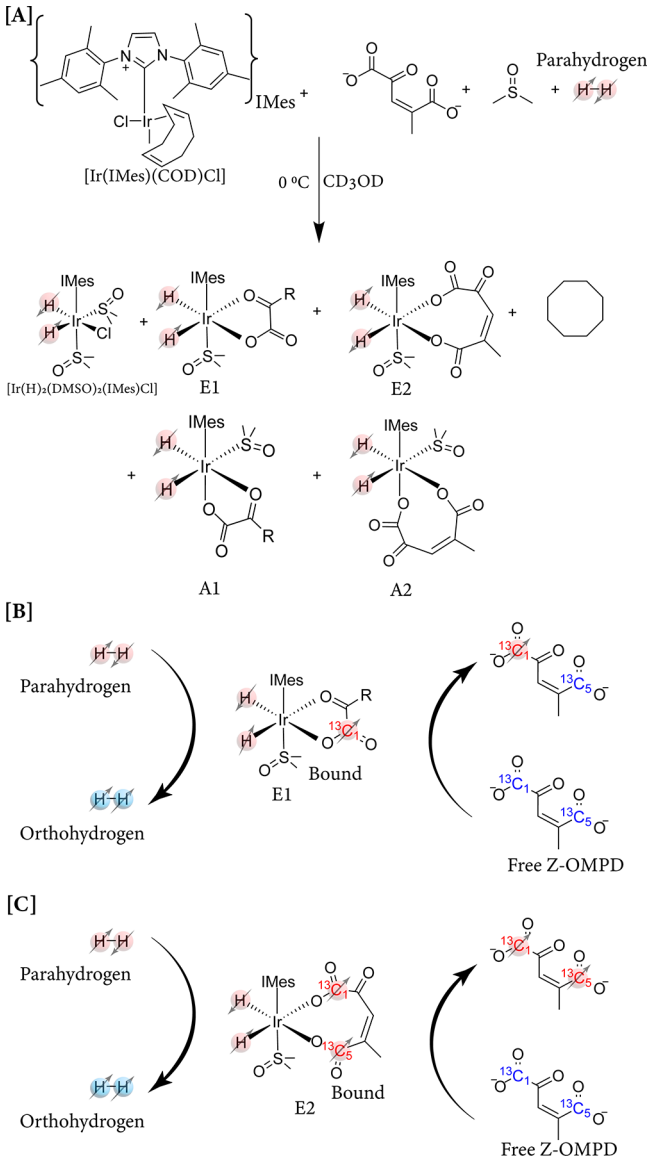

(pyruvate as the substrate), **A1** and **E1** correspond to **3a** and **3b**, respectively, as introduced in previous work.[67] Assuming only **A1** and **E1** complexes are formed, the labeled C-1 position is expected to be the main target of polarization since C-5 is not directly bound to the iridium complex in these configurations, as illustrated in Scheme 1b. However, our experimental observations with Z-OMPD show significant polarization in both C-1 and C-5 (though P_{13C} for C-1 is 1.6× higher), as shown in Figure 1B. This result implies that Z-OMPD also exhibits other coordination modes such as **A2** and **E2** in contrast to pyruvate or other alpha-keto acids.[72,73] We hypothesize that the **E2** complex in which both C-1 and C-5

https://doi.org/10.1021/acssensors.4c01102
ACS Sens. XXXX, XXX, XXX−XXX

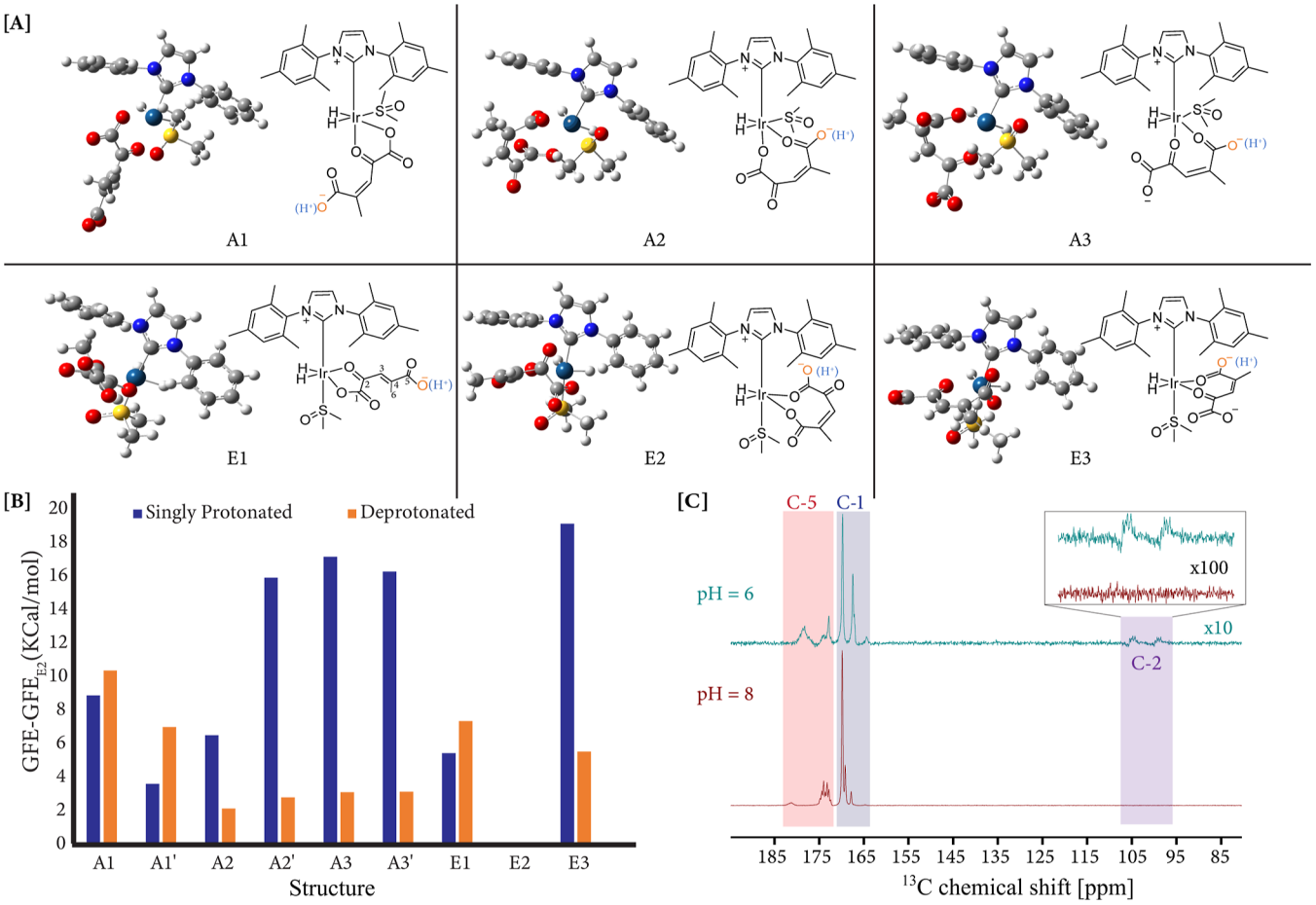

Figure 2. (A) Three-dimensional structures of the optimized geometry of axial complexes **A1**−**A3** and equatorial complexes **E1**−**E3**. (B) Plot of relative energies of structures **A1**−**A3**, **A1′**−**A3′**, and **E1**−**E3** with respect to **E2** for both the deprotonated and singly protonated state of Z-OMPD. (C) HP spectra of Z-OMPD at pH 6 and pH 8, showing that unlabeled C-2 is polarized at lower pH (singly protonated state), therefore suggesting that the **E1** complex is significantly present at lower pH.

coordinate with the iridium center of the catalyst is responsible for C-1 and C-5 hyperpolarization, as illustrated in Scheme 1c. To determine which complexes are responsible for the SABRE spin order transfer (SOT), we carried out DFT calculations on nine possible binding modes of Z-OMPD to the catalyst to compare their relative energies. The optimized geometries of six complexes are presented in Figure 2A (see Figure S3 for the full set). Out of the six, the first three are the axial complexes **A1**, **A2**, and **A3** (their inverse **A1′**, **A2′**, and **A3′** are shown in the Supporting Information). **A1** (and **A1′**) is formed when Z-OMPD binds axially via the oxo groups at positions C-1 and C-2. **A2** (and **A2′**) binding occurs at positions C-1 and C-5, while **A3** (and **A3′**) binding occurs at C-2 and C-5 positions. The remaining three complexes **E1**, **E2**, and **E3** are the equatorial analogues of the axial complexes. The relative energy of each complex is presented in Figure 2B. Each Z-OMPD complex was optimized for both the fully deprotonated carboxylates (at C-1 and C-5) and the singly deprotonated carboxylate (at C-1). In computing the relative Gibbs free energies, we set the lowest energy for each protonation state to be zero because a direct comparison between these two sets of complexes is challenging given that they have different number of atoms. It should be noted that at high pH (specifically 8.42) where the hyperpolarization is performed, Z-OMPD exists as the dianion (fully deprotonated), and at lower pH (between 3 and 6), it exists as the monoanion (singly deprotonated). In this lower pH range, only the carboxylate at C-1 is deprotonated.

Interestingly, the **E2** configuration has the lowest relative energy in comparison to all other complexes for both the dianion (pH > 6.5) and monoanion (pH < 6.5). The **A2** complex is also relatively stable for the dianion complex. The relative stabilities of the **E2** and **A2** complexes indicate a direct binding of the carboxylate groups at positions C-1 and C-5, consistent with the experimental results. This finding can also be rationalized by the fact that C-1 and C-5 are the most electro-negative groups where electron density is the highest, enabling more favorable interactions with the Ir center. Furthermore, when the experiment was performed at pH 6, where Z-OMPD is singly deprotonated at the C-1 position, we observed an overall reduction in signal intensity at both C-1 and C-5. This observation is consistent with the assumption that **E2** is the primary driver of polarization transfer, which becomes destabilized at pH < 6.5, when the electron density is reduced at C-5 due to proton binding.

Relative to **E2**, the **E1** and **A1′**complexes are slightly favored in the singly deprotonated state compared to the fully deprotonated state as shown in Figure S3A (relative energies of **E1** and **A1′** are 5.458 and 3.624 kcal/mol for singly deprotonated compared to 7.372 and 7.011 kcal/mol for fully deprotonated). The slight increase in the relative stability of **E1** and **A1′** at pH 6 explains our experimental observation, shown

https://doi.org/10.1021/acssensors.4c01102
ACS Sens. XXXX, XXX, XXX−XXX

in Figure 2C, where polarization at the unlabeled C-2 position is observed at pH 6, whereas at pH 8, no C-2 polarization is detected. It should be noted that for singly deprotonated Z-OMPD complexes, **A1′** is energetically favored compared to **E1**; however, axial complexes (such as **A1′**) contain spin topology that do not allow for efficient polarization transfer.[70,74] Although more studies are still necessary to determine the identity of all of the SABRE-active Z-OMPD complexes, the evidence discussed above suggests that **E2** and **E1** are the primary active SABRE complexes, where **E2** drives the SABRE process at high pH (∼8) and a combination of **E2** and **E1** drives SABRE at lower pH (∼6).

To further understand the SABRE dynamics of Z-OMPD, the temperature dependence of the C-1 and C-5 polarizations was examined in a series of temperature cycling experiments with varying initial temperature of the sample. (Details about the temperature of the sample as a function of bubbling time and initial temperature was published previously.[59]) The results are presented in Figure 3A,B. At the lowest initial temperature investigated (−15 °C), the catalyst-bound C-1 peak dominates the spectrum as the exchange rate between catalyst bound and free Z-OMPD is limited; however, at higher temperatures (15 °C), exchange is too fast to allow effective SOT, and consequently, both free and bound species have considerably lower polarization.[42,59,72,75,76] The optimum initial temperature was found to be between 0 and 5 °C. At this optimal precooling temperature, efficient polarization of the bound species occurs at appropriate hydride exchange rates, while the Z-OMPD remains bound. Then, as the sample warms, Z-OMPD exchanges into the free form more efficiently, ultimately leading to high levels of polarization for the free C-1 and C-5 carbons.

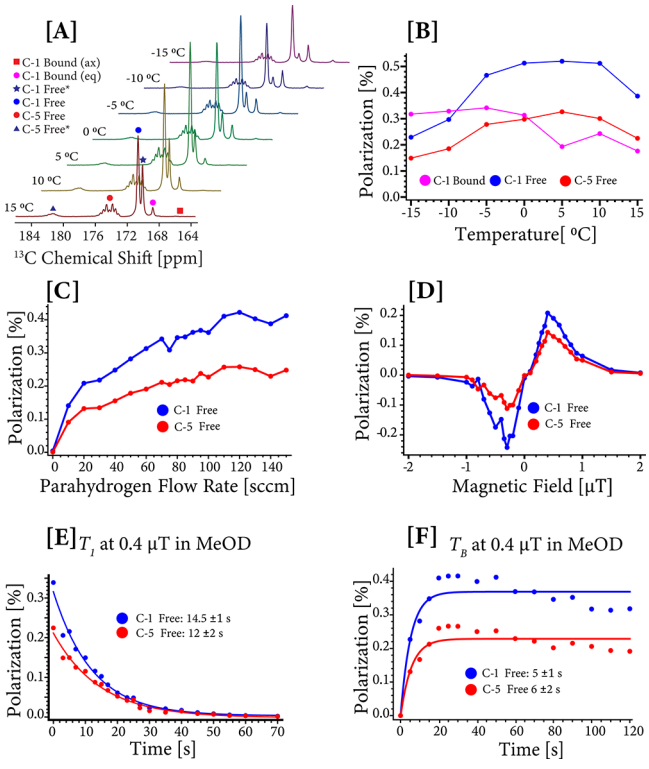

Figure 3. Optimization study. (A) ^{13}C HP spectra of [1,5-$^{13}C_2$]Z-OMPD at initial temperatures ranging from −15 to 15 °C. (B) Plot of percent polarization against initial temperature for free C-1 (blue), bound C-1 (magenta), and free C-5 (red). (C) pH_2 flow rate dependence of Z-OMPD polarization, varied from 0 to 15 sccm at 100 psi. (D) Field dependence of Z-OMPD polarization. (E) T_1 relaxation study of HP Z-OMPD at 0.4 μT fitted with a simple exponential decay curve. The data were collected by bubbling the sample for 30 s at 0.4 μT and varying the delay time. (F) Polarization buildup on free Z-OMPD for both C-1 and C-5. Data acquired by varying the pH_2 bubbling time.

It should be noted that we do not observe the bound C-5 peak likely due to the faster dissociation rates of the carboxylate group at C-5 compared to that of the carboxylate group at C-1. This is consistent with the idea that the alpha-keto acids alternate between the bidentate form (coordination with both carboxylates at C-1 and C-5) and monodentate form (coordination with carboxylate at C-1 alone) to promote pH_2 exchange.[54] This hopping mechanism between the two forms likely explains why only the bound C-1 peak is observed. For future advances in Z-OMPD hyperpolarization, it will be crucial to precisely determine the exchange rate of Z-OMPD and the hydrides, which we were not able to quantify at this time.

To further improve the polarization on Z-OMPD with SABRE-SHEATH, the dependence on the pH_2 flow rate was examined. Polarization buildup is dependent on the amount of fresh pH_2 in solution, which is regulated by the pressure and flow rate of pH_2. Our current experimental setup is limited to 100 psi; therefore, we investigated polarization as a function of the flow rate at that pressure.

As presented in Figure 3C, we note an increase in polarization with increasing flow rate, consistent with previous studies using the pyruvate system.[47] The highest P_{13C} for both free C-1 and C-5 Z-OMPD was achieved at a flow rate of 120 sccm. Above 120 sccm, we note a slight drop in the polarization due to the sample experiencing a wider range of magnetic fields in the SABRE-SHEATH setup as it moves up the NMR tube, decreasing magnetic field homogeneity and, consequently, SOT efficiency.

Next, to transfer polarization to Z-OMPD using SABRE-SHEATH, the frequency difference between the hydrides and the C-1 and C-5 carbons of Z-OMPD must match the hydride−hydride J-coupling.[39,40,43,77] This matching is achieved through careful optimization of the magnetic field sensed by the nuclei in the μT range (measured using a Twinleaf magnetometer). Figure 3D shows the polarization of C-1 and C-5 as a function of the PTF. The negative fields correspond to magnetic fields that are inverted relative to the spectrometer field. The inverse field produces inverted HP magnetization (see Figure S4). The maximum P_{13C} for both free C-1 and C-5 is observed at ∼0.4 μT.

Another important parameter of HP substrates is the T_1 relaxation time. Accordingly, we conducted a T_1 relaxation study at 0.4 μT shown in Figure 3E. This study was conducted by bubbling through the sample for 30 s, followed by a variable time delay (0−70 s) with the sample placed in the 0.4 μT field before detection. As seen from Figure 3E, Z-OMPD exhibits fast relaxation at microtesla fields (14.5 ± 1 s at C-1 and 12 ± 2 s at C-5). The relaxation is due to intra- and intermolecular interactions with other NMR active nuclei in Z-OMPD and on the catalyst.[58,78] Specifically, at 0.4 μT, the J-coupling network that is responsible for building up hyperpolarization in the first place will also cause relaxation when bubbling is halted. In contrast, at intermediate fields where these interactions are less dominant, Z-OMPD shows significantly longer T_1 relaxation

https://doi.org/10.1021/acssensors.4c01102
ACS Sens. XXXX, XXX, XXX−XXX

times (@1T in D_2O: C-1 T_1 = 138 ± 26 s; C-5 T_1 = 119 ± 1 s) as reported by Grashei et al.,[38] which is very promising for future applications.

Finally, the polarization buildup on Z-OMPD was studied by varying the bubbling time (0−120 s) at 0.4 μT (Figure 3F). Again, the experiments were conducted as temperature cycling experiments where the sample was precooled to 5 °C and bubbling was performed at RT such that the sample experienced a temperature gradient during the bubbling time. The buildup data presented in Figure 3F were fit by a simple exponential buildup curve. We observed a decay in polarization at later bubbling times, which is expected in temperature cycling experiments because temperatures of the sample rise with bubbling time, leading to increased exchange rates that are too fast for efficient polarization transfer. Under the present experimental conditions, Z-OMPD has a rapid polarization buildup (C-1 T_B = 5 ± 1 s; C-5 T_B = 6 ± 2 s). The fast buildup and relatively quick relaxation of Z-OMPD at 0.4 μT explain the limited level of polarization achieved on both C-1 and C-5 carbons of Z-OMPD. Further optimization would require the mitigation of the factors that lead to fast relaxation; this may be achieved in the future through deuteration of both Z-OMPD and the catalyst, in conjunction with polarization transfer methods that also work at elevated fields such as alt-SABRE,[79] LIGHT-SABRE,[54] SLIC-SABRE,[55] etc.

pH Sensing. To showcase the pH sensing ability of HP Z-OMPD, the frequency difference between C-1 and C-5 was monitored as a function of pH. The pH adjustment was carried out as follows. First, polarization was performed as described above; then, the sample was transferred to a storage field of 0.5 T (using a permanent Halbach array magnet) where the sample was depressurized, and 0.5 mL of buffer were added. A citrate-phosphate buffer was used for pH 3.08−7.6, and a sodium carbonate-bicarbonate buffer was used for pH 8.30−11.14. Finally, the detection was performed on a 1.1 T benchtop NMR instrument under proton decoupling. As seen in Figure 4A, we note an increasing chemical shift difference between C-1 and C-5 as pH increases. Specifically, with increasing pH, the chemical shift of C-5 increases, whereas the chemical shift of C-1 slightly decreases. C-5 is more sensitive to pH changes compared to C-1 because C-5 is closer to the site which exhibits a change in protonation across this pH regime.[38,80] The difference between chemical shifts of C-1 and C-5 ($\Delta\delta_{C\text{-}5,\ C\text{-}1}$) as a function of pH shows approximately a ~3 ppm shift across the examined pH range (3.80−11.14). In Figure 4B, $\Delta\delta_{C\text{-}5,\ C\text{-}1}$, is plotted against pH.[38] The data were fit to the modified Henderson−Hasselbalch equation

$$\mathrm{pH} = \mathrm{p}K_a + \log\left(\frac{\Delta\delta_{c5,c1(\mathrm{observed})} - \Delta\delta_{c5,c1(\mathrm{protonated})}}{\Delta\delta_{c5,c1(\mathrm{deprotonated})} - \Delta\delta_{c5,c1(\mathrm{observed})}}\right) \quad (1)$$

In the fitting routine using eq 1, p*K*a is a fitting parameter and a value of $\mathrm{p}K_a$ = 7.05 is extracted. This is different from the previously reported value of $\mathrm{p}K_a$ = 6.55 in D_2O.[38] The difference is likely a result of using a methanolic solvent as opposed to water. The use of a chemical shift difference, $\Delta\delta_{C\text{-}5,\ C\text{-}1}$, as opposed to a single chemical shift, is particularly significant as it eliminates the need for an external standard for pH sensing, positioning HP Z-OMPD as a unique pH sensor.

The data displayed in Figure 4A also reveal a pH-dependent $^{13}C-^{13}C$ *J*-coupling. At pH values above 6.5, the decoupled ^{13}C peaks appear as singlets, whereas at pH values below 6.5,

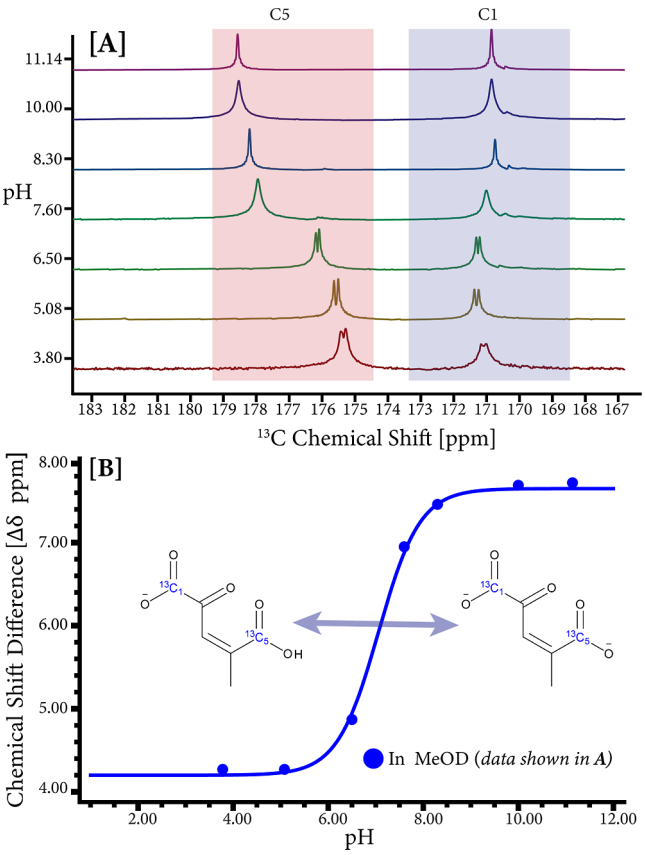

Figure 4. Chemical shift difference between C-5 and C-1 of Z-OMPD dianion as a function of pH. (A) ^{13}C NMR decoupled spectra of HP Z-OMPD at a pH range between 3.80 and 11.14. The hyperpolarization was always performed at pH 8. (B) Plot of chemical shift difference of C-1 and C-5 as a function of pH.

the doublets are recognizable, which are split by $^{13}C-^{13}C$ *J*-couplings on the order of 1.5 Hz. Interestingly, close examination of the splitting shows slightly increasing *J*-coupling values with a decreasing pH. (We also provide analogous data acquired without decoupling in Figure S5.)

CONCLUSIONS

In conclusion, we have demonstrated the feasibility of hyperpolarizing Z-OMPD at both C-1 and C-5 positions simultaneously with SABRE-SHEATH. We have studied the likely binding modes of Z-OMPD to the hyperpolarization catalyst by experiment and DFT calculations. The work revealed that there is more than one possible binding mode of Z-OMPD to the catalyst. Particularly, at elevated pH (>6.5), the equatorial complex **E2** is mostly responsible for hyperpolarization, whereas at lower pH (<6.5), a combination of **E1** and **E2** is found to contribute to the polarization. This study highlights the role of bidentate binding in the form of five-membered (**E1**) and eight-membered (**E2**) rings, which presents unique research opportunities in SABRE dynamics and chemistry, widening the utilization of SABRE to substrates with similar moieties that were previously unamenable to SABRE hyperpolarization.

We also showed the important role that temperature, flow rate, and polarization-transfer field play in the optimization of polarization levels. One important finding is that the relaxation rates at 0.4 μT are relatively fast (~12 s at C-1 and 14.5 s at C-5) as compared to relaxation rates at higher fields (138 and

https://doi.org/10.1021/acssensors.4c01102
ACS Sens. XXXX, XXX, XXX−XXX

119 s at 1 T), which indicates that polarization levels can likely be improved significantly with polarization transfer methods that work at higher fields.[54,56,79]

Finally, the enhanced signal was used to demonstrate the utility of Z-OMPD as a pH sensor. Over the pH range from pH 3.08 to pH 11.14, the chemical shift difference between C-1 and C-5 changes by 3 ppm, and we used a pH-dependent fitting model to extract the pK_a value of 7.05.

Compared to other hyperpolarization methods, the technology package of SABRE offers fast, scalable, and inexpensive production of HP agents. The possibility of preparing HP Z-OMPD with SABRE may provide new opportunities in the development of noninvasive assessment of extracellular pH by HP MRI using simpler hyperpolarization technology. In this first study, the polarization levels remained modest below 1%. This is similar to the first hyperpolarization levels for pyruvate when first established as a SABRE substrate, which subsequently was optimized to exceed 20%.[55,59,67,70] Accordingly, we are hopeful that similarly high polarization levels will be enabled on Z-OMPD in the future. After improving the polarization levels, it will also be critical to achieve biocompatibility, which could be accomplished by emerging purification protocols.[50,71,81,82]

■ ASSOCIATED CONTENT

Supporting Information

The Supporting Information is available free of charge at https://pubs.acs.org/doi/10.1021/acssensors.4c01102.

Polarization calculation and coordinates of DFT optimized structures (PDF)

■ AUTHOR INFORMATION

Corresponding Authors

Mustapha B. Abdulmojeed − *Department of Chemistry, North Carolina State University, Raleigh, North Carolina 27695, United States;* orcid.org/0000-0002-5513-3658; Email: mbabdulm@ncsu.edu

Thomas Theis − *Department of Chemistry, North Carolina State University, Raleigh, North Carolina 27695, United States; Department of Physics, North Carolina State University, Raleigh, North Carolina 27695, United States;* orcid.org/0000-0001-6779-9978; Email: ttheis@ncsu.edu

Authors

Martin Grashei − *Technical University of Munich, School of Medicine and Health, Department of Nuclear Medicine, TUM University Hospital, D-81675 Munich, Germany*

Seth Dilday − *Department of Chemistry, North Carolina State University, Raleigh, North Carolina 27695, United States*

Pascal Wodtke − *Technical University of Munich, School of Medicine and Health, Department of Nuclear Medicine, TUM University Hospital, D-81675 Munich, Germany;* orcid.org/0000-0002-6109-4261

Stephen McBride − *Department of Chemistry, North Carolina State University, Raleigh, North Carolina 27695, United States*

Atli Davidsson − *Department of Chemistry, North Carolina State University, Raleigh, North Carolina 27695, United States*

Erica Curran − *Department of Chemistry, North Carolina State University, Raleigh, North Carolina 27695, United States*

Keilian MacCulloch − *Department of Chemistry, North Carolina State University, Raleigh, North Carolina 27695, United States;* orcid.org/0000-0002-4506-5057

Austin Browning − *Department of Chemistry, North Carolina State University, Raleigh, North Carolina 27695, United States;* orcid.org/0000-0001-9190-1215

Patrick TomHon − *Vizma Life Sciences, Chapel Hill, North Carolina 27514, United States*

Andreas B. Schmidt − *Division of Medical Physics, Department of Radiology, University Medical Center Freiburg, Faculty of Medicine, University of Freiburg, Freiburg 79106, Germany; German Cancer Consortium (DKTK), Partner Site Freiburg, German Cancer Research Center (DKFZ), Heidelberg 69120, Germany; Department of Chemistry, Integrated Biosciences (Ibio), Wayne State University, Karmanos Center Institute (KCI), Detroit, Michigan 48202, United States;* orcid.org/0000-0001-8944-7463

Eduard Y. Chekmenev − *Department of Chemistry, Integrated Biosciences (Ibio), Wayne State University, Karmanos Center Institute (KCI), Detroit, Michigan 48202, United States;* orcid.org/0000-0002-8745-8801

Franz Schilling − *Technical University of Munich, School of Medicine and Health, Department of Nuclear Medicine, TUM University Hospital, D-81675 Munich, Germany; German Cancer Consortium (DKTK), Partner Site Munich, German Cancer Research Center (DKFZ), Heidelberg 69120, Germany;* orcid.org/0000-0001-5239-4628

Complete contact information is available at: https://pubs.acs.org/10.1021/acssensors.4c01102

Author Contributions

The manuscript was written through contributions of all authors. All authors have given approval to the final version of the manuscript.

Notes

The authors declare the following competing financial interest(s): Thomas Theis and Patrick TomHon hold stock in Vizma Life Sciences LLC (VLS). VLS is developing products related to the research being reported. Patrick TomHon serves as Chief Scientific Officer (CSO) of VLS. Thomas Theis serves as the Chair of the Scientific Advisory Board of VLS. The terms of this arrangement have been reviewed and approved by NC State University in accordance with its policy on objectivity in research. Eduard Y. Chekmenev discloses a stake of ownership in XeUS Technologies Ltd., and VLS. Eduard Chekmenev serves on the Scientific Advisory Board of VLS.

■ ACKNOWLEDGMENTS

Research reported in this publication was supported by the National Institute of Biomedical Imaging and Bioengineering of the National Institutes of Health under award nos. NIH R21EB025313, NIH R01EB029829, and R21EB033872. The content is solely the responsibility of the authors and does not necessarily represent the official views of the National Institutes of Health. In addition, we acknowledge funding from the Mallinckrodt Foundation, the National Science Foundation under award no. NSF CHE-1904780 and NSF

CHE-2404387, the North Carolina Biotechnology Center in the form of a Translational Research Grant. A.B.S. and F.S. would like to thank the German Cancer Consortium; A.B.S. also thanks the German Research Foundation (SCHM 3694/1-1, SCHM 3694/2-1, and SFB1479) and the German Federal Ministry of Education and Research (BMBF) in the funding program "Quantum Technologies-from Basic Research to Market" under the project "QuE-MRT" (contract number: 13N16448). Finally, we would like to acknowledge the support from NCSU's METRIC in providing access to NMR instrumentation. This material is based upon work supported by the U.S. Department of Energy, Office of Biological and Environmental Research (BER) under award number DE-SC0023334. Disclaimer: "This report was prepared as an account of work sponsored by an agency of the United States Government. Neither the United States Government nor any agency thereof, nor any of their employees, makes any warranty, express or implied, or assumes any legal liability or responsibility for the accuracy, completeness, or usefulness of any information, apparatus, product, or process disclosed, or represents that its use would not infringe privately owned rights. Reference herein to any specific commercial product, process, or service by trade name, trademark, manufacturer, or otherwise does not necessarily constitute or imply its endorsement, recommendation, or favoring by the United States Government or any agency thereof. The views and opinions of authors expressed herein do not necessarily state or reflect those of the United States Government or any agency.

■ ABBREVIATIONS

HP	hyperpolarized
Z-OMPD	*Z*-4-methyl-2-oxopent-3-enedioic acid;
SABRE-SHEATH	signal amplification by reversible exchange in SHield enabling alignment transfer to heteronuclei
MR	magnetic resonance

■ REFERENCES

(1) Vaupel, P.; Kallinowski, F.; Okunieff, P. Blood Flow, Oxygen and Nutrient Supply, and Metabolic Microenvironment of Human Tumors: A Review. *Cancer Res.* **1989**, *49* (23), 6449−6465.
(2) Tannock, I. F.; Rotin, D. Acid PH in Tumors and Its Potential for Therapeutic Exploitation. *Cancer Res.* **1989**, *49* (16), 4373−4384.
(3) Gerweck, L. E.; Seetharaman, K. Cellular PH Gradient in Tumor versus Normal Tissue: Potential Exploitation for the Treatment of Cancer. *Cancer Res.* **1996**, *56* (6), 1194−1198.
(4) Martin, G. R.; Jain, R. K. Noninvasive Measurement of Interstitial PH Profiles in Normal and Neoplastic Using Fluorescence Ratio Imaging Microscopy. *Cancer Res.* **1994**, *54* (21), 5670−5674.
(5) Griffiths, J. R. Are Cancer Cells Acidic? *Br. J. Cancer* **1991**, *64*, 425−427.
(6) Lee, S. H.; Griffiths, J. R. How and Why Are Cancers Acidic? Carbonic Anhydrase Ix and the Homeostatic Control of Tumour Extracellular Ph. *Cancers* **2020**, *12* (6), 1616.
(7) Thews, O.; Riemann, A. Tumor PH and Metastasis: A Malignant Process beyond Hypoxia. *Cancer Metastasis Rev.* **2019**, *38* (1−2), 113−129.
(8) Jokivarsi, K. T.; Gröhn, H. I.; Gröhn, O. H.; Kauppinen, R. A. Proton Transfer Ratio, Lactate, and Intracellular PH in Acute Cerebral Ischemia. *Magn. Reson. Med.* **2007**, *57* (4), 647−653.
(9) Gorodetsky, A. A.; Kirilyuk, I. A.; Khramtsov, V. V.; Komarov, D. A. Functional Electron Paramagnetic Resonance Imaging of Ischemic Rat Heart: Monitoring of Tissue Oxygenation and PH. *Magn. Reson. Med.* **2016**, *76* (1), 350−358.
(10) Longo, D. L.; Cutrin, J. C.; Michelotti, F.; Irrera, P.; Aime, S. Noninvasive Evaluation of Renal PH Homeostasis after Ischemia Reperfusion Injury by CEST-MRI. *NMR Biomed.* **2017**, *30* (7), No. e3720.
(11) Bruno, C. M.; Valenti, M. Acid-Base Disorders in Patients with Chronic Obstructive Pulmonary Disease: A Pathophysiological Review. *J. Biomed. Biotechnol.* **2012**, *2012*, 1−8.
(12) Kurtzman, N. A. Renal Tubular Acidosis Syndromes. *South Med. J.* **2000**, *93* (11), 1042−1052.
(13) Huber, V.; Camisaschi, C.; Berzi, A.; Ferro, S.; Lugini, L.; Triulzi, T.; Tuccitto, A.; Tagliabue, E.; Castelli, C.; Rivoltini, L. Cancer Acidity: An Ultimate Frontier of Tumor Immune Escape and a Novel Target of Immunomodulation. *Seminars in Cancer Biology*. Academic Press April 1, 2017; pp 74−89. DOI: .
(14) Wang, B. Y.; Zhang, J.; Wang, J. L.; Sun, S.; Wang, Z. H.; Wang, L. P.; Zhang, Q. L.; Lv, F. F.; Cao, E. Y.; Shao, Z. M.; Fais, S.; Hu, X. C. Intermittent High Dose Proton Pump Inhibitor Enhances the Antitumor Effects of Chemotherapy in Metastatic Breast Cancer. *J. Exp. Clin. Cancer Res.* **2015**, *34* (1), 85.
(15) Nakagawa, Y.; Negishi, Y.; Shimizu, M.; Takahashi, M.; Ichikawa, M.; Takahashi, H. Effects of Extracellular PH and Hypoxia on the Function and Development of Antigen-Specific Cytotoxic T Lymphocytes. *Immunol. Lett.* **2015**, *167* (2), 72−86.
(16) Jardim-Perassi, B. V.; Irrera, P.; Oluwatola, O. E.; Abrahams, D.; Estrella, V. C.; Ordway, B.; Byrne, S. R.; Ojeda, A. A.; Whelan, C. J.; Kim, J.; Beatty, M. S.; Damgaci-Erturk, S.; Longo, D. L.; Gaspar, K. J.; Siegers, G. M.; Centeno, B. A.; Lau, J. Y. C.; Pilon-Thomas, S. A.; Ibrahim-Hashim, A.; Gillies, R. J. L-DOS47 Elevates Pancreatic Cancer Tumor PH and Enhances Response to Immunotherapy. *Biomedicines* **2024**, *12* (2), 461.
(17) Irrera, P.; Roberto, M.; Consolino, L.; Anemone, A.; Villano, D.; Navarro-Tableros, V.; Carella, A.; Dastrù, W.; Aime, S.; Longo, D. L. Effect of Esomeprazole Treatment on Extracellular Tumor PH in a Preclinical Model of Prostate Cancer by MRI-CEST Tumor PH Imaging. *Metabolites* **2022**, *13* (1), 48.
(18) Dhakan, C.; Anemone, A.; Ventura, V.; Carella, A.; Corrado, A.; Pirotta, E.; Villano, D.; Romdhane, F.; Gammaraccio, F.; Aime, S.; Longo, D. L. Assessing the Therapeutic Efficacy of Proton Transport Inhibitors in a Triple-Negative Breast Cancer Murine Model with Magnetic Resonance Imaging—Chemical Exchange Saturation Transfer Tumor PH Imaging. *Metabolites* **2023**, *13* (11), 1161.
(19) Pilon-Thomas, S.; Kodumudi, K. N.; El-Kenawi, A. E.; Russell, S.; Weber, A. M.; Luddy, K.; Damaghi, M.; Wojtkowiak, J. W.; Mulé, J. J.; Ibrahim-Hashim, A.; Gillies, R. J. Neutralization of Tumor Acidity Improves Antitumor Responses to Immunotherapy. *Cancer Res.* **2016**, *76* (6), 1381−1390.
(20) Kim, H.; Krishnamurthy, L. C.; Sun, P. Z. Brain PH Imaging and Its Applications. *Neuroscience* **2021**, *474*, 51−62.
(21) Gillies, R. J.; Raghunand, N.; Garcia-Martin, M. L.; Gatenby, R. A. PH maging A Review of PH Measurement Methods and Applications in Cancers. *IEEE Eng. Med. Biol. Mag.* **2004**, *23* (5), 57−64.
(22) Gillies, R. J.; Raghunand, N.; Garcia-Martin, M. L.; Gatenby, R. A. PH Imaging. *IEEE Eng. Med. Biol. Magazine* **2004**, *23*, 57−64.
(23) Anemone, A.; Consolino, L.; Arena, F.; Capozza, M.; Longo, D. L. Imaging Tumor Acidosis: A Survey of the Available Techniques for Mapping in Vivo Tumor PH. *Cancer Metastasis Rev.* **2019**, *38* (1−2), 25−49.
(24) Chen, J.; Hackett, E. P.; Singh, J.; Kovács, Z.; Park, J. M. Simultaneous Assessment of Intracellular and Extracellular PH Using Hyperpolarized [1−13C]Alanine Ethyl Ester. *Anal. Chem.* **2020**, *92* (17), 11681−11686.
(25) Hashim, A. I.; Zhang, X.; Wojtkowiak, J. W.; Martinez, G. V.; Gillies, R. J. Imaging PH and Metastasis. *NMR Biomed.* **2011**, *24* (6), 582−591.
(26) Gillies, R. J.; Bhujwalla, Z.; Liu, Z. 31P-MRS Measurements of Extracellular PH of Tumors Using 3 = aminomomdx > homhonate. *Am. J. Physiol.* **1994**, *267* (1), C195-203.

https://doi.org/10.1021/acssensors.4c01102
ACS Sens. XXXX, XXX, XXX−XXX

(27) García-Martín, M.-L.; Hérigault, G.; Rémy, C.; Farion, R.; Ballesteros, P.; Coles, J. A.; Cerdán, S.; Ziegler, A. Mapping Extracellular PH in Rat Brain Gliomas in Vivo by 1 H Magnetic Resonance Spectroscopic Imaging: Comparison with Maps of Metabolites 1. *Cancer Res.* **2001**, *61* (17), 6524−6531. http://aacrjournals.org/cancerres/article-pdf/61/17/6524/2486551/ch1701006524.pdf

(28) Gillies, R. J.; Liu, Z.; Bhujwalla, Z. 31P-MRS Measurements of Extracellular PH of Tumors Using 3- Aminopropylphosphonate. *Am. J. Physiol.: Cell Physiol.* **1994**, *267* (1), C195−C203.

(29) Chen, L. Q.; Pagel, M. D. Evaluating PH in the Extracellular Tumor Microenvironment Using CEST MRI and Other Imaging Methods. *Adv. Radiol.* **2015**, *2015*, 1−25.

(30) García-Martín, M.-L.; Hérigault, G.; Rémy, C.; Farion, R.; Ballesteros, P.; Coles, J. A.; Cerdán, S.; Ziegler, A. Mapping Extracellular PH in Rat Brain Gliomas in Vivo by 1H Magnetic Resonance Spectroscopic Imaging: Comparison with Maps of Metabolites 1. *Cancer Res.* **2001**, *61* (17), 6524−6531.

(31) Gil, S.; Zaderenzo, P.; Cruz, F.; Cerdan, S.; Ballesteros, P. Imidazole-1-Ylalkanoic Acids as Extrinsic 1H NMR Probes for the Determination of Intracellular PH, Extracellular PH and Cell Volume. *Bioorg. Med. Chem.Bioorg. Med. Chem.* **1994**, *2* (5), 305−314.

(32) Halse, M. E. Perspectives for Hyperpolarisation in Compact NMR. *TrAC, Trends Anal. Chem.* **2016**, *83*, 76−83.

(33) Ardenkjaer-Larsen, J. H.; Boebinger, G. S.; Comment, A.; Duckett, S.; Edison, A. S.; Engelke, F.; Griesinger, C.; Griffin, R. G.; Hilty, C.; Maeda, H.; Parigi, G.; Prisner, T.; Ravera, E.; van Bentum, J.; Vega, S.; Webb, A.; Luchinat, C.; Schwalbe, H.; Frydman, L. Facing and Overcoming Sensitivity Challenges in Biomolecular NMR Spectroscopy. *Angew. Chem., Int. Ed.* **2015**, *54* (32), 9162−9185.

(34) Nikolaou, P.; Goodson, B. M.; Chekmenev, E. Y. NMR Hyperpolarization Techniques for Biomedicine. *Chem.—Eur. J.* **2015**, *21* (8), 3156−3166.

(35) Korenchan, D. E.; Taglang, C.; Von Morze, C.; Blecha, J. E.; Gordon, J. W.; Sriram, R.; Larson, P. E. Z.; Vigneron, D. B.; Vanbrocklin, H. F.; Kurhanewicz, J.; Wilson, D. M.; Flavell, R. R. Dicarboxylic Acids as PH Sensors for Hyperpolarized 13C Magnetic Resonance Spectroscopic Imaging. *Analyst* **2017**, *142* (9), 1429−1433.

(36) Düwel, S.; Hundshammer, C.; Gersch, M.; Feuerecker, B.; Steiger, K.; Buck, A.; Walch, A.; Haase, A.; Glaser, S. J.; Schwaiger, M.; Schilling, F. Imaging of PH in Vivo Using Hyperpolarized 13C-Labelled Zymonic Acid. *Nat. Commun.* **2017**, *8* (1), 15126.

(37) Flavell, R. R.; Von Morze, C.; Blecha, J. E.; Korenchan, D. E.; Van Criekinge, M.; Sriram, R.; Gordon, J. W.; Chen, H. Y.; Subramaniam, S.; Bok, R. A.; Wang, Z. J.; Vigneron, D. B.; Larson, P. E.; Kurhanewicz, J.; Wilson, D. M. Application of Good's Buffers to PH Imaging Using Hyperpolarized 13C MRI. *Chem. Commun.* **2015**, *51* (74), 14119−14122.

(38) Grashei, M.; Wodtke, P.; Skinner, J. G.; Sühnel, S.; Setzer, N.; Metzler, T.; Gulde, S.; Park, M.; Witt, D.; Mohr, H.; Hundshammer, C.; Strittmatter, N.; Pellegata, N. S.; Steiger, K.; Schilling, F. Simultaneous Magnetic Resonance Imaging of PH, Perfusion and Renal Filtration Using Hyperpolarized 13C-Labelled Z-OMPD. *Nat. Commun.* **2023**, *14* (1), 5060.

(39) Truong, M. L.; Theis, T.; Coffey, A. M.; Shchepin, R. V.; Waddell, K. W.; Shi, F.; Goodson, B. M.; Warren, W. S.; Chekmenev, E. Y. 15N Hyperpolarization by Reversible Exchange Using SABRE-SHEATH. *J. Phys. Chem. C* **2015**, *119* (16), 8786−8797.

(40) Theis, T.; Truong, M. L.; Coffey, A. M.; Shchepin, R. V.; Waddell, K. W.; Shi, F.; Goodson, B. M.; Warren, W. S.; Chekmenev, E. Y. Microtesla SABRE Enables 10% Nitrogen-15 Nuclear Spin Polarization. *J. Am. Chem. Soc.* **2015**, *137* (4), 1404−1407.

(41) Adams, R. W.; Aguilar, J. A.; Atkinson, K. D.; Cowley, M. J.; Elliott, P. I. P.; Duckett, S. B.; Green, G. G. R.; Khazal, i. G.; López-Serrano, J.; Williamson, D. C. Reversible Interactions with Para-Hydrogen Enhance NMR Sensitivity by Polarization Transfer. *Science* **2009**, *323* (5922), 1708−1711.

(42) Cowley, M. J.; Adams, R. W.; Atkinson, K. D.; Cockett, M. C. R.; Duckett, S. B.; Green, G. G. R.; Lohman, J. A. B.; Kerssebaum, R.; Kilgour, D.; Mewis, R. E. Iridium N-Heterocyclic Carbene Complexes as Efficient Catalysts for Magnetization Transfer from Para -Hydrogen. *J. Am. Chem. Soc.* **2011**, *133* (16), 6134−6137.

(43) Ivanov, K. L.; Pravdivtsev, A. N.; Yurkovskaya, A. V.; Vieth, H. M.; Kaptein, R. The Role of Level Anti-Crossings in Nuclear Spin Hyperpolarization. *Prog. Nucl. Magn. Reson. Spectrosc.* **2014**, *81*, 1−36.

(44) Hövener, J.; Pravdivtsev, A. N.; Kidd, B.; Bowers, C. R.; Glöggler, S.; Kovtunov, K. V.; Plaumann, M.; Katz-Brull, R.; Buckenmaier, K.; Jerschow, A.; Reineri, F.; Theis, T.; Shchepin, R. V.; Wagner, S.; Bhattacharya, P.; Zacharias, N. M.; Chekmenev, E. Y. Parahydrogen-Based Hyperpolarization for Biomedicine. *Angew. Chem., Int. Ed.* **2018**, *57* (35), 11140−11162.

(45) Green, R. A.; Adams, R. W.; Duckett, S. B.; Mewis, R. E.; Williamson, D. C.; Green, G. G. R. The Theory and Practice of Hyperpolarization in Magnetic Resonance Using Parahydrogen. *Prog. Nucl. Magn. Reson. Spectrosc.* **2012**, *67* (November), 1−48.

(46) Colell, J. F. P.; Logan, A. W. J.; Zhou, Z.; Shchepin, R. V.; Barskiy, D. A.; Ortiz, G. X.; Wang, Q.; Malcolmson, S. J.; Chekmenev, E. Y.; Warren, W. S.; Theis, T. Generalizing, Extending, and Maximizing Nitrogen-15 Hyperpolarization Induced by Parahydrogen in Reversible Exchange. *J. Phys. Chem. C* **2017**, *121* (12), 6626−6634.

(47) Barskiy, D. A.; Knecht, S.; Yurkovskaya, A. V.; Ivanov, K. L. SABRE: Chemical Kinetics and Spin Dynamics of the Formation of Hyperpolarization. *Prog. Nucl. Magn. Reson. Spectrosc.* **2019**, *114*−*115*, 33−70.

(48) Fear, E. J.; Kennerley, A. J.; Rayner, P. J.; Norcott, P.; Roy, S. S.; Duckett, S. B. SABRE Hyperpolarized Anticancer Agents for Use in 1H MRI. *Magn. Reson. Med.* **2022**, *88*, 11−27.

(49) Kovtunov, K. V.; Pokochueva, E. V.; Salnikov, O. G.; Cousin, S. F.; Kurzbach, D.; Vuichoud, B.; Jannin, S.; Chekmenev, E. Y.; Goodson, B. M.; Barskiy, D. A.; Koptyug, I. V. Hyperpolarized NMR Spectroscopy: D-DNP, PHIP, and SABRE Techniques. *Chem.−Asian J.* **2018**, *13* (15), 1857−1871.

(50) Kidd, B. E.; Gesiorski, J. L.; Gemeinhardt, M. E.; Shchepin, R. V.; Kovtunov, K. V.; Koptyug, I. V.; Chekmenev, E. Y.; Goodson, B. M. Facile Removal of Homogeneous SABRE Catalysts for Purifying Hyperpolarized Metronidazole, a Potential Hypoxia Sensor. *J. Phys. Chem. C* **2018**, *122* (29), 16848−16852.

(51) Albers, M. J.; Bok, R.; Chen, A. P.; Cunningham, C. H.; Zierhut, M. L.; Zhang, V. Y.; Kohler, S. J.; Tropp, J.; Hurd, R. E.; Yen, Y. F.; Nelson, S. J.; Vigneron, D. B.; Kurhanewicz, J. Hyperpolarized 13C Lactate, Pyruvate, and Alanine: Noninvasive Biomarkers for Prostate Cancer Detection and Grading. *Cancer Res.* **2008**, *68* (20), 8607−8615.

(52) Miloushev, V. Z.; Granlund, K. L.; Boltyanskiy, R.; Lyashchenko, S. K.; DeAngelis, L. M.; Mellinghoff, I. K.; Brennan, C. W.; Tabar, V.; Yang, T. J.; Holodny, A. I.; Sosa, R. E.; Guo, Y. W. W.; Chen, A. P.; Tropp, J.; Robb, F.; Keshari, K. R. Metabolic Imaging of the Human Brain with Hyperpolarized 13C Pyruvate Demonstrates 13C Lactate Production in Brain Tumor Patients. *Cancer Res.* **2018**, *78* (14), 3755−3760.

(53) Cavallari, E.; Carrera, C.; Sorge, M.; Bonne, G.; Muchir, A.; Aime, S.; Reineri, F. The 13C Hyperpolarized Pyruvate Generated by ParaHydrogen Detects the Response of the Heart to Altered Metabolism in Real Time. *Sci. Rep.* **2018**, *8* (1), 8366.

(54) Pravdivtsev, A. N.; Buckenmaier, K.; Kempf, N.; Stevanato, G.; Scheffler, K.; Engelmann, J.; Plaumann, M.; Koerber, R.; Hövener, J. B.; Theis, T. LIGHT-SABRE Hyperpolarizes 1−13C-Pyruvate Continuously without Magnetic Field Cycling. *J. Phys. Chem. C* **2023**, *127* (14), 6744−6753.

(55) Schmidt, A. B.; Eills, J.; Dagys, L.; Gierse, M.; Keim, M.; Lucas, S.; Bock, M.; Schwartz, I.; Zaitsev, M.; Chekmenev, E. Y.; Knecht, S. Over 20% Carbon-13 Polarization of Perdeuterated Pyruvate Using Reversible Exchange with Parahydrogen and Spin-Lock Induced Crossing at 50 MT. *J. Phys. Chem. Lett.* **2023**, *14* (23), 5305−5309.

(56) Knecht, S.; Kiryutin, A. S.; Yurkovskaya, A. V.; Ivanov, K. L. Efficient Conversion of Anti-Phase Spin Order of Protons into 15N

https://doi.org/10.1021/acssensors.4c01102
ACS Sens. XXXX, XXX, XXX−XXX

Magnetisation Using SLIC-SABRE. *Mol. Phys.* **2019**, *117* (19), 2762−2771.
(57) Rios, A. C.; Bera, P. P.; Moreno, J. A.; Cooper, G. Pyruvate Aldol Condensation Product: A Metabolite That Escaped Synthetic Preparation for over a Century. *ACS Omega* **2020**, *5* (25), 15063−15068.
(58) Adelabu, I.; TomHon, P.; Kabir, M. S. H.; Nantogma, S.; Abdulmojeed, M.; Mandzhieva, I.; Ettedgui, J.; Swenson, R. E.; Krishna, M. C.; Theis, T.; Goodson, B. M.; Chekmenev, E. Y. Order-Unity 13C Nuclear Polarization of [1−13C]Pyruvate in Seconds and the Interplay of Water and SABRE Enhancement. *ChemPhysChem* **2022**, *23* (2), No. e202100839.
(59) Tomhon, P.; Abdulmojeed, M.; Adelabu, I.; Nantogma, S.; Kabir, M. S. H.; Lehmkuhl, S.; Chekmenev, E. Y.; Theis, T. Temperature Cycling Enables Efficient 13C SABRE-SHEATH Hyperpolarization and Imaging of [1−13C]-Pyruvate. *J. Am. Chem. Soc.* **2022**, *144* (1), 282−287.
(60) Notes, U.; References, U.; Boese, A. D.; Handy, N. C.; Cammi, R.; Cappelli, C.; Corni, S.; Tomasi, J.; Clemente, F.; Vreven, T.; Frisch, M. J.; Collins, M. A.; Fukui, K.; Henderson, T. M.; Izmaylov, A. F.; Scalmani, G.; Scuseria, G. E.; Izmaylov, A. F.; Scuseria, G.; Frisch, M. J.; Marenich, A. V.; Cramer, C. J.; Truhlar, D. G. *Gaussian 09* Revision B. 01 Release Notes. 2010, *125* (August), 8−11.
(61) Stephens, P. J.; Devlin, F. J.; Chabalowski, C. F.; Frisch, M. J. Ab Initio Calculation of Vibrational Absorption and Circular Dichroism Spectra Using Density Functional Force Fields. *J. Phys. Chem.* **1994**, *98* (45), 11623−11627.
(62) Vosko, S. H.; Wilk, L.; Nusair, M. Accurate Spin-Dependent Electron Liquid Correlation Energies for Local Spin Density Calculations: A Critical Analysis. *Can. J. Phys.* **1980**, *58* (8), 1200−1211.
(63) Lee, C.; Yang, W.; Parr, R. G. Development of the Colle-Salvetti Correlation-Energy Formula into a Functional of the Electron Density. *Phys. Rev. B* **1988**, *37* (2), 785−789.
(64) Becke, A. D. Density-functional Thermochemistry. III. The Role of Exact Exchange. *J. Chem. Phys.* **1993**, *98* (7), 5648−5652.
(65) Ehlers, A. W.; Böhme, M.; Dapprich, S.; Gobbi, A.; Höllwarth, A.; Jonas, V.; Köhler, K. F.; Stegmann, R.; Veldkamp, A.; Frenking, G. A Set of F-Polarization Functions for Pseudo-Potential Basis Sets of the Transition Metals Sc-Cu, Y-Ag and La-Au. *Chem. Phys. Lett.* **1993**, *208* (1−2), 111−114.
(66) Ditchfield, R.; Hehre, W. J.; Pople, J. A. Self-Consistent Molecular-Orbital Methods. IX. An Extended Gaussian-Type Basis for Molecular-Orbital Studies of Organic Molecules. *J. Chem. Phys.* **1971**, *54* (2), 724−728.
(67) Iali, W.; Roy, S. S.; Tickner, B. J.; Ahwal, F.; Kennerley, A. J.; Duckett, S. B. Hyperpolarising Pyruvate through Signal Amplification by Reversible Exchange (SABRE). *Angew. Chem.* **2019**, *131* (30), 10377−10381.
(68) Tickner, B. J.; Rayner, P. J.; Duckett, S. B. Using SABRE Hyperpolarized 13C NMR Spectroscopy to Interrogate Organic Transformations of Pyruvate. *Anal. Chem.* **2020**, *92* (13), 9095−9103.
(69) Pravdivtsev, A. N.; Buckenmaier, K.; Kempf, N.; Stevanato, G.; Scheffler, K.; Engelmann, J.; Plaumann, M.; Koerber, R.; Hövener, J. B.; Theis, T. LIGHT-SABRE Hyperpolarizes 1−13C-Pyruvate Continuously without Magnetic Field Cycling. *J. Phys. Chem. C* **2023**, *127* (14), 6744−6753.
(70) Tickner, B. J.; Semenova, O.; Iali, W.; Rayner, P. J.; Whitwood, A. C.; Duckett, S. B. Optimisation of Pyruvate Hyperpolarisation Using SABRE by Tuning the Active Magnetisation Transfer Catalyst. *Catal. Sci. Technol.* **2020**, *10* (5), 1343−1355.
(71) MacCulloch, K.; Browning, A.; Guarin Bedoya, D. O.; McBride, S. J.; Abdulmojeed, M. B.; Dedesma, C.; Goodson, B. M.; Rosen, M. S.; Chekmenev, E. Y.; Yen, Y.-F.; TomHon, P.; Theis, T. Facile Hyperpolarization Chemistry for Molecular Imaging and Metabolic Tracking of [1−13C]Pyruvate in Vivo. *J. Magn. Reson. Open* **2023**, *16−17* (July), 100129.
(72) Adelabu, I.; Ettedgui, J.; Joshi, S. M.; Nantogma, S.; Chowdhury, M. R. H.; McBride, S.; Theis, T.; Sabbasani, V. R.; Chandrasekhar, M.; Sail, D.; Yamamoto, K.; Swenson, R. E.; Krishna, M. C.; Goodson, B. M.; Chekmenev, E. Y. Rapid 13C Hyperpolarization of the TCA Cycle Intermediate α-Ketoglutarate via SABRE-SHEATH. *Anal. Chem.* **2022**, *94* (39), 13422−13431.
(73) Adelabu, I.; Chowdhury, M. R. H.; Nantogma, S.; Oladun, C.; Ahmed, F.; Stilgenbauer, L.; Sadagurski, M.; Theis, T.; Goodson, B. M.; Chekmenev, E. Y. Efficient SABRE-SHEATH Hyperpolarization of Potent Branched-Chain-Amino-Acid Metabolic Probe [1−13C]-Ketoisocaproate. *Metabolites* **2023**, *13* (2), 200.
(74) Tickner, B. J.; Lewis, J. S.; John, R. O.; Whitwood, A. C.; Duckett, S. B. Mechanistic Insight into Novel Sulfoxide Containing SABRE Polarisation Transfer Catalysts. *Dalton Trans.* **2019**, *48* (40), 15198−15206.
(75) Tickner, B. J.; Ahwal, F.; Whitwood, A. C.; Duckett, S. B. Reversible Hyperpolarization of Ketoisocaproate Using Sulfoxide-Containing Polarization Transfer Catalysts. *ChemPhysChem* **2021**, *22* (1), 13−17.
(76) Hövener, J.; Knecht, S.; Schwaderlapp, N.; Hennig, J.; Von Elverfeldt, D. Continuous Re-Hyperpolarization of Nuclear Spins Using Parahydrogen: Theory and Experiment. *ChemPhysChem* **2014**, *15* (12), 2451−2457.
(77) Buljubasich, L.; Franzoni, M. B.; Spiess, H. W.; Münnemann, K. Level Anti-Crossings in ParaHydrogen Induced Polarization Experiments with Cs-Symmetric Molecules. *J. Magn. Reson.* **2012**, *219*, 33−40.
(78) Schmidt, A. B.; De Maissin, H.; Adelabu, I.; Nantogma, S.; Ettedgui, J.; Tomhon, P.; Goodson, B. M.; Theis, T.; Chekmenev, E. Y. Catalyst-Free Aqueous Hyperpolarized [1−13C]Pyruvate Obtained by Re-Dissolution Signal Amplification by Reversible Exchange. *ACS Sens.* **2022**, *7* (11), 3430−3439.
(79) Pravdivtsev, A. N.; Kempf, N.; Plaumann, M.; Bernarding, J.; Scheffler, K.; Hövener, J.; Buckenmaier, K. Coherent Evolution of Signal Amplification by Reversible Exchange in Two Alternating Fields (Alt-SABRE). *ChemPhysChem* **2021**, *22* (23), 2381−2386.
(80) Köcher, S. S.; Düwel, S.; Hundshammer, C.; Glaser, S. J.; Schilling, F.; Granwehr, J.; Scheurer, C. Ab Initio Simulation of PH-Sensitive Biomarkers in Magnetic Resonance Imaging. *J. Phys. Chem. A* **2018**, *122* (40), 7983−7990.
(81) de Maissin, H.; Groß, P. R.; Mohiuddin, O.; Weigt, M.; Nagel, L.; Herzog, M.; Wang, Z.; Willing, R.; Reichardt, W.; Pichotka, M.; Heß, L.; Reinheckel, T.; Jessen, H. J.; Zeiser, R.; Bock, M.; von Elverfeldt, D.; Zaitsev, M.; Korchak, S.; Glöggler, S.; Glöggler, S.; Chekmenev, E. Y.; Schilling, F.; Knecht, S.; Schmidt, A. B.; de Maissin, H.; Groß, P. R.; Mohiuddin, O.; Weigt, M.; Herzog, M.; Wang, Z.; Willing, R.; Reichardt, W.; Pichotka, M.; Bock, M.; von Elverfeldt, D.; Zaitsev, M.; Schmidt, A. B.; Nagel, L.; Schilling, F.; Heß, L.; Reinheckel, T.; Jessen, H. J.; Zeiser, R.; Korchak, S.; Glöggler, S.; Hövener, J.; Chekmenev, E. Y.; Knecht, S. In Vivo Metabolic Imaging of [1-^{13}C]Pyruvate-d_3 Hyperpolarized By Reversible Exchange With Parahydrogen**. *Angew. Chem. Int. Ed.* **2023**, *62*, 202306654−202306655.
(82) Schmidt, A. B.; De Maissin, H.; Adelabu, I.; Nantogma, S.; Ettedgui, J.; Tomhon, P.; Goodson, B. M.; Theis, T.; Chekmenev, E. Y. Catalyst-Free Aqueous Hyperpolarized [1−13C]Pyruvate Obtained by Re-Dissolution Signal Amplification by Reversible Exchange. *ACS Sens.* **2022**, *7* (11), 3430−3439.

https://doi.org/10.1021/acssensors.4c01102
ACS Sens. XXXX, XXX, XXX−XXX